Vibrational spectroscopy and microwave dielectric properties of $AY_2Si_3O_{10}$ (A=Sr, Ba) ceramics for 5G applications

Qianbi Lin,[a] Kaixin Song,[*,a,f] Bing Liu,[a] Hadi Barzegar Bafrooei[a], Di Zhou[b], Weitao Su[c], Feng Shi[d], Dawei Wang[*f], Huixin Lin[*e], Ian M.Reaney[f]

[a]College of electronic information, Hangzhou Dianzi University, Hangzhou, 310018, Zhejiang, China

[b]Electronic Materials Research Laboratory, Key Laboratory of the Ministry of Education & International Center for Dielectric Research, Xi'an Jiaotong University, Xi'an, 710049, Shanxi, China

[c]College of Materials Sciences and Environmental Engineering, Hangzhou Dianzi University, Hangzhou, 310018, Zhejiang, China

[d]Department of materials sciences and engineering, Shandong university of sciences and technology, Qingdao, 266590, Shandong, China

[e]Shanghai Institute of Ceramics, Chinese Academy of Sciences, Shanghai, 200050, China

[f]Department of Materials Science and Engineering, The University of Sheffield, Sheffield, S13JD, U.K,

Abstract

$AY_2Si_3O_{10}$ (A=Sr, Ba) trisilicate ceramics were synthesized by traditional high temperature solid state reaction method. X-ray diffraction patterns and Rietveld refinement revealed that $AY_2Si_3O_{10}$ (A=Sr, Ba) ceramics belonged to triclinic and monoclinic crystal systems with $P\bar{1}$ and $P2_1/m$ space groups, respectively. The vibrational modes of $[SiO_4]$ tetrahedra, $[YO_6]$ octahedra and $[(Sr/Ba)O_8]$ polyhedra were analyzed by Raman spectroscopy. The infrared spectroscopy fitting analysis was used to determine intrinsic dielectric properties. Excellent microwave dielectric properties were measured for $SrY_2Si_3O_{10}$ and $BaY_2Si_3O_{10}$ with ε_r = 9.3, Qf =

* Corresponding author. Kaixin Song, kxsong@hdu.edu.cn; Huixing Lin, linhuixing@mail.sic.ac.cn; Dawei Wang, dawei.wang@sheffield.ac.uk.

64100GHz, τ_f = -31ppm/°C and ε_r = 9.5, Qf = 65600GHz, τ_f = -28ppm/°C, respectively. Both trisilicate ceramics are considered potential candidates for 5G and mm wave technology, provided τ_f can be further tuned.

Key words: Low permittivity, IR spectra, Raman spectroscopy, 5G ceramics

Introduction

5th generation (5G) telecommunications will become the dominant wireless protocol in the next 10 years for applications such as mobile phones, WIFI, global positioning systems, Intelligent Transport Systems and the Internet of Things.[1-3] According to the world wireless society, the assigned working frequency bands for 5G are ultimately 24 - 30 GHz or 60 GHz -70 GHz with delay time of signal transmission < 1ms.[4] Unlike 2G/3G/4G mobile communications, the carrier frequency of 5G is extended to millimeter wave band rather than microwave band, which has enormous implications for the development of microwave dielectrics. Since the delay time is proportional to the square root of dielectric permittivity (ε_r), the radio signal propagation velocity can be increased by using dielectrics with low ε_r.[5] Furthermore, high quality factor (Qf) is required to decrease energy loss with near zero temperature coefficients of resonant frequency (τ_f) paramount to maintain operating stability.[6-7]

In the past few years, several kinds of low ε_r ceramics have been reported, such as silicates, molybdates, and borates, often focusing on their use as low temperature co-fired ceramics (LTCC).[8-10] Most low ε_r (< 10) materials are silicates, due to the strong covalent Si-O bond in [SiO_4] tetrahedroa.[11] Many silicate ceramics with [SiO_4] tetrahedra have been reported such as Mg_2SiO_4,[12] Zn_2SiO_4,[13] $LiAlSiO_4$,[14] $CaSnSiO_5$,[15] Al_2SiO_5,[16] $Mg_2Al_4Si_5O_{18}$,[17] $CaMgSi_2O_6$ [18] and are summarized in Table 1.

Table 1. The microwave dielectric properties of some silicate ceramics reported in references.

Silicate Ceramics	Q×f(GHz)	ε_r	τ_f(ppm/°C)	Ref
Mg_2SiO_4	240000	6.8	-65	12
Zn_2SiO_4	219000	6.6	-61	13
$LiAlSiO_4$	36000	4.8	8	14

$CaSnSiO_5$	61000	9.1	35	15
Al_2SiO_5	41800	4.4	-17	16
$Mg_2Al_4Si_5O_{18}$	39000	6.3	-32	17
$CaMgSi_2O_6$	53000	8.3	-45	18
$SrY_2Si_3O_{10}$	64100	9.3	-31	This work
$BaY_2Si_3O_{10}$	65600	9.5	-28	This work

Silicates with the trisilicate structure contain isolated $[Si_3O_{10}]$ units, which also are accompanied by additional $[SiO_4]$ or $[SiO_7]$ units such as $R_2Si_2O_7$(R = Gd, Tb, Dy, Ho)[19] or protonated variants $Si_3O_8(OH)_2$ groups such as $Ca_3[Si_3O_8(OH)_2]$.[20] In 1976, Povarennykh et al.[21] summarized 17 natural and synthetic trisilicate compounds with structural characteristics of $SrY_2Si_3O_{10}$ and $BaY_2Si_3O_{10}$ additionally reported by Kolitsch and Wierzbicka et al.[22,23] The effect of doping with rare earth ions on the luminescence properties and energy conversion of $BaY_2Si_3O_{10}$ has been studied by Xia et al,[24] but to our knowledge, the microwave dielectric properties of $AY_2Si_3O_{10}$ (A=Sr, Ba) trisilicate ceramics has not been reported.

In this work, pure $AY_2Si_3O_{10}$ (A=Sr, Ba) ceramics were successfully prepared via a conventional solid-state reaction method. The nominal compound of $CaY_2Si_3O_{10}$ could not be synthesized in our experiments. The evolution of crystal structure, grain morphology and vibrational lattice modes as well as the microwave dielectric properties are systematically investigated.

1. Experimental

The $AY_2Si_3O_{10}$ (A=Sr, Ba) ceramics were fabricated using high-purity oxide powders $SrCO_3$ (99.5%) Y_2O_3 (99.9%), $BaCO_3$ (99.8%) SiO_2 (99.99%) as raw materials. Raw materials were weighed according to the nominal stoichiometric compositions and ball-milled 24 h in ethanol using zirconia media. After the mixture was dried at 90°C, it was calcined in air at 1250°C for 4 h at a heating rate of 4°C/min. The calcined powder was re-milled, dried again and pressed into 10 mm diameter, 6 mm high pellets at 100MPa. The samples were sintered at 1300°C–1450°C for 4h.

The bulk densities of as sintered samples were measured by the Archimedes method. The room temperature crystalline phase constituents were identified by X-ray powder diffraction (XRD, RIGAKU D/max 2550/PC, Rigaku Co., Tokyo, Japan) using Cu K radiation(λ=0.154056 nm) radiation at a voltage of 40 kV and current of 30 mA. Rietveld refinement of the XRD patterns was carried out using general structure analysis system (GSAS) software.[25] The thermal etched surfaces of $AY_2Si_3O_{10}$ (A=Sr, Ba) ceramic were characterized using a scanning electron microscopy (SEM，Sirion 200，Netherlands). The Raman spectra were collected at room temperature using a Raman spectrometer (LabRAM HR800) excited with an Ar^+ laser (514.5 nm). Far-infrared reflectivity spectra were obtained between 50-5000 cm^{-1} using a Bruker IFS 66v FT-IR spectrometer at the Infrared Spectroscopy and Micro-spectroscopy Endstation (BL01B) at the National Synchrotron Radiation Lab (NSRL) Hefei, China. ε_r and Qf were measured using the parallel plate method [26] with a vector network analyzer (E8363，Agilent Technologies Inc. Santa Clara, CA, USA). τ_f was measured in a temperature range of 20°C-80°C and calculated by the following equation:

$$\tau_f = \frac{1}{f(T_0)} \frac{[f(T_1) - f(T_0)]}{T_1 - T_0} \times 10^6 \text{ ppm/}^{o}\text{C} \qquad (1)$$

Where, $f(T_1)$ and $f(T_0)$ represent the resonant frequency at T_1 (80°C) and T_0 (20°C), respectively.

2. Results and discussion

The XRD patterns of the $SrY_2Si_3O_{10}$ and $BaY_2Si_3O_{10}$ ceramics powders are shown in Fig. 1(a) and (c), respectively, without detectable secondary phase. Both phase compositions match well with $SrY_2Si_3O_{10}$ and $BaY_2Si_3O_{10}$ (ICSD cards No:167613 and 240470), respectively. The refined profiles of both samples by the Rietveld method based on GSAS software are given in Fig. 1 (b) and (d). Where tricinic ($P\bar{1}$) and monoclinic ($P2_1/m$) crystal structure are used separately, low refinement factors, R_{wp} = 6.99%, R_p = 5.11%, χ^2 = 3.134 for $SrY_2Si_3O_{10}$ and R_{wp} = 10.75%, R_p = 7.72%, χ^2=4.529 for $BaY_2Si_3O_{10}$, are obtained, indicating good

agreement between the observed and calculated patterns. The calculated lattice parameters are a = 6.751173Å, b = 6.876599Å, c = 9.259163Å, V = 409.266Å^3 for $SrY_2Si_3O_{10}$ and a = 5.378373Å, b = 12.207029Å, c = 6.844245Å, V = 431.059Å^3 for $BaY_2Si_3O_{10}$. The refined structure parameters are listed in Table 2 and Table 3, and the schematic crystal structures of $AY_2Si_3O_{10}$ (A=Sr, Ba) are depicted in the insert of Fig. 1(b) and (d).

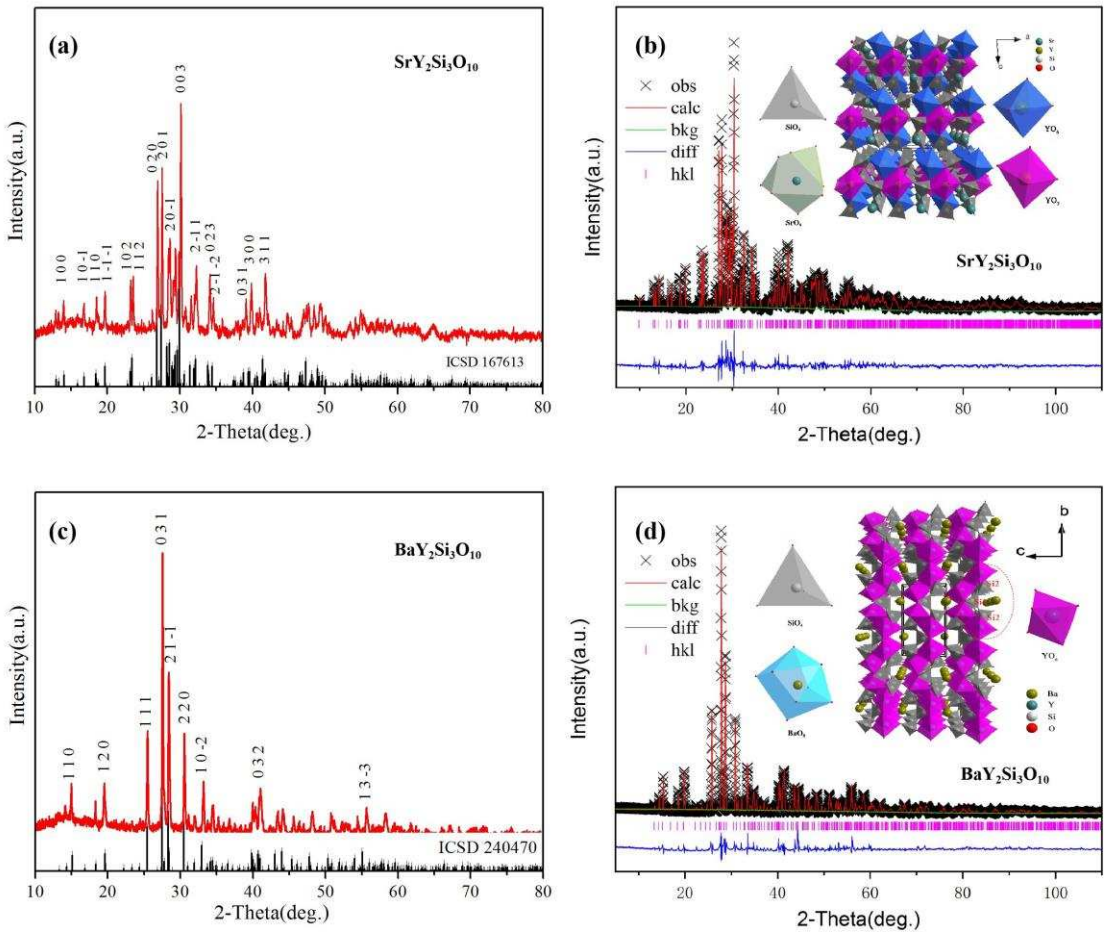

Fig.1, XRD patterns and Rietveld refinement results of $AY_2Si_3O_{10}$ (A=Sr, Ba) ceramics samples. (a, b) $SrY_2Si_3O_{10}$ and (c, d) $BaY_2Si_3O_{10}$ ceramics sintered at 1425°C for 4 hours; the schematic crystal structure of $SrY_2Si_3O_{10}$ and $BaY_2Si_3O_{10}$ are given in the inset of (b) and (d), respectively.

Table 2. Atomic positions of $SrY_2Si_3O_{10}$ ceramic sample refined by the Rietveld refinement.

Atom	x	y	z	Occupancy	Uiso
Sr1	0.399825	1.094081	0.179838	1	0.00803
Y1	0.139754	0.753070	0.512454	1	0.00539
Y2	0.156582	0.259501	0.810740	1	0.00603
Si1	-0.333027	0.721909	0.542101	1	0.00477
Si2	-0.334922	0.368323	0.831899	1	0.00482

Si3	0.122786	0.743093	0.878762	1	0.00546
O1	0.472250	0.786072	0.471154	1	0.00920
O2	0.187039	0.403048	0.537943	1	0.00720
O3	0.188117	1.112924	0.426797	1	0.00760
O4	0.389787	1.418450	0.288936	1	0.00870
O5	0.475927	0.228399	0.875362	1	0.00760
O6	0.171245	0.763830	0.249256	1	0.00810
O7	0.267720	0.384419	0.985231	1	0.01120
O8	0.095678	0.205811	1.054879	1	0.00970
O9	0.231999	-0.047554	0.777292	1	0.00130
O10	0.114035	0.621938	0.762843	1	0.00770

Table 3. Atomic positions of $BaY_2Si_3O_{10}$ ceramic sample refined by the Rietveld refinement.

Atom	x	y	z	Occupancy	Uiso
Ba1	0.760820	0.250000	0.019920	1	0.00954
Y1	0.158010	0.098858	0.684310	1	0.00637
Si1	0.582420	0.250000	0.489170	1	0.00570
Si2	0.303790	0.062050	0.213440	1	0.00579
O1	0.372300	0.250000	0.615800	1	0.00780
O2	0.876600	0.250000	0.634400	1	0.00690
O3	0.548300	0.142870	0.339700	1	0.01050
O4	0.430800	-0.054550	0.190700	1	0.01050
O5	0.165200	0.123470	0.00300	1	0.01070
O6	0.100200	0.051920	0.351100	1	0.00880

SEM images of $AY_2Si_3O_{10}$ (A=Sr, Ba) ceramics sintered at different temperatures are shown in Fig. 2. Due to low crystal symmetry, pillar or plate-shaped grains of $SrY_2Si_3O_{10}$ and $BaY_2Si_3O_{10}$ are observed in both samples. The grain sizes increased gradually with reducing porosity as a function of sintering temperature with dense and compact microstructures obtained. However, the crystal particles of $SrY_2Si_3O_{10}$ begin to abnormally growing up from above 1450 ^oC.

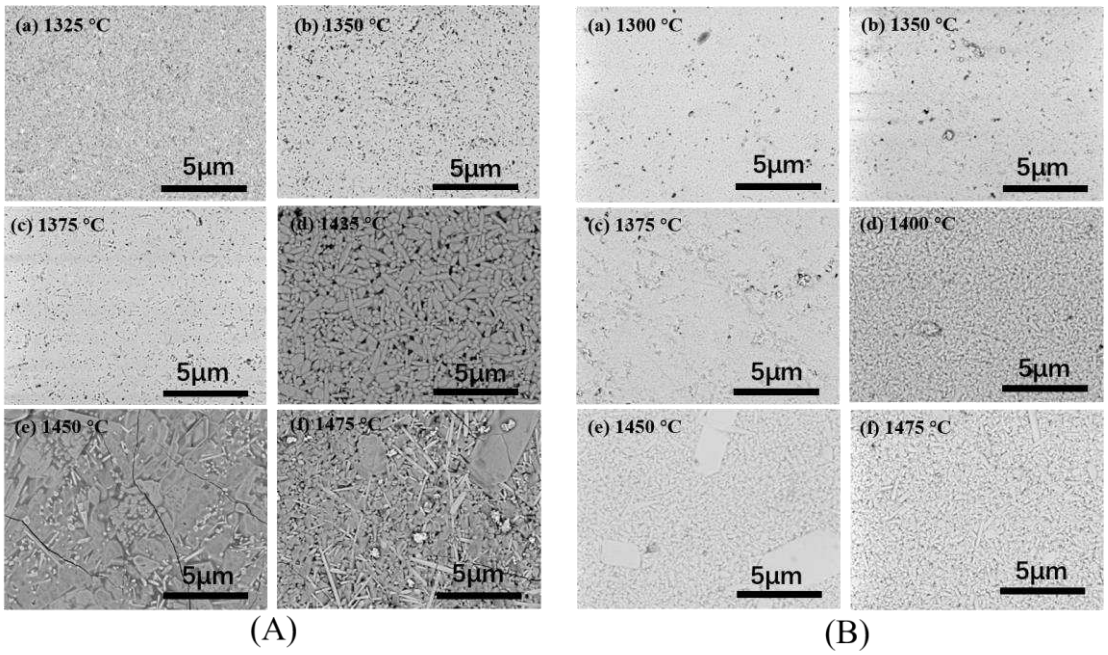

Fig.2 , (A) The thermal etched surface of SEM images of the $SrY_2Si_3O_{10}$ ceramics: (a) 1325°C, (b) 1350°C, (c) 1375°C, (d) 1425°C, (e)1450°C and (f) 1475°C; (B) The thermal etched suface of SEM images of the $BaY_2Si_3O_{10}$ ceramics: (a) 1300°C, (b) 1350°C,(c) 1375°C, (d) 1400°C, (e)1450°C and (f) 1475°C.

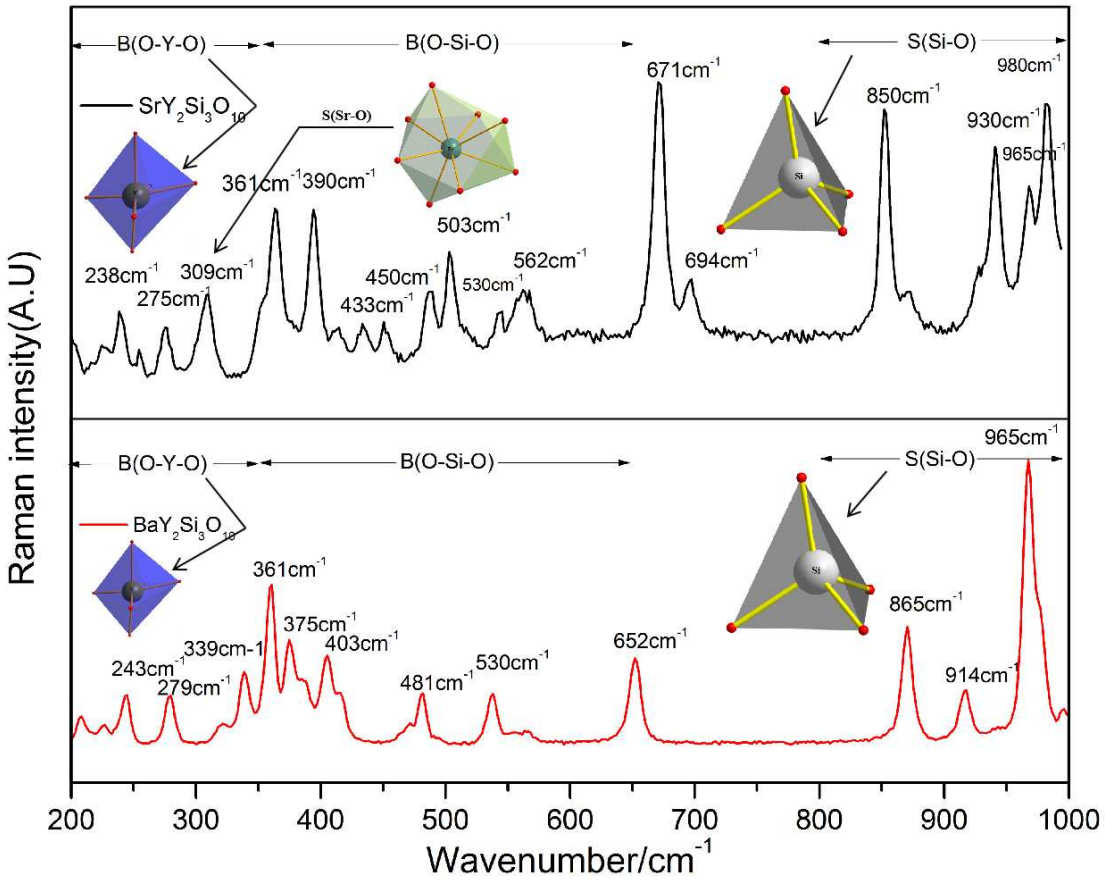

Fig. 3, Observed Raman spectra of $AY_2Si_3O_{10}$ (A=Sr, Ba) ceramics.

The Raman spectra of $AY_2Si_3O_{10}$ (A=Sr, Ba) are given in Fig. 3 and the corresponding Raman active modes are described as $48A_g$ for $SrY_2Si_3O_{10}$ and $26A_g+22B_g$ for $BaY_2Si_3O_{10}$, respectively, which are obtained from online software that provides group factor and symmetry analysis.[27] Not all vibrational modes may be recognized due to mode overlap or coupling. The vibration modes of most silicates can be divided into three types as a function of wavenumber, as presented in Fig. 3. [28, 29] 800-1000cm^{-1} is attributed to S(Si-O) stretching modes, 350-800cm^{-1} is dominated by B(O-Si-O) bending modes and 200-350cm^{-1} is related to B(O-Y-O) bending modes. The observed (Obs) Raman vibrational mode types are listed in Table 4.

Table 4. The vibration modes of observed Raman peaks in $BaY_2Si_3O_{10}$ and $SrY_2Si_3O_{10}$ ceramics (S: stretching, B: bending)

$BaY_2Si_3O_{10}$		$SrY_2Si_3O_{10}$	
Obs(cm^{-1})	Vibration type	Obs(cm^{-1})	Vibration type
0-200	(Ba-O)	224	B(O-Y-O)
207	B(O-Y-O),B(Y-O),BS(Y-Y)	238	B(O-Y-O)
226	B(O-Y-O)	275	S(O-Y-O)
243	B(O-Y-O)	309	S(Sr-O)
279	B(O-Y-O)	361	B(Y-Si-O)
339	B(O-Y-O), B(Y-O)	390	S(O-Si-O)
361	B(Y-Si-O)	412	S(O-Y-O), B(O-Si-O)
375	B(O-Si-O), BS(Y-Si-O)	433	B(Si-O-Y)
403	B(O-Si-O)	450	B(O-Si-O)
481	B(O-Si-O)	503	B(Si-O-Si)
530	B(Y-Si-O)	530	B(Y-Si-O)
652	B(O-Si-O)	562	B(O-Si-O)
865	S(Si-O)	671	B(Y-Si-O)
914	S(Si-O)	694	S(Si-Si)
965	S(Si-O)	850	S(Si-O)
		930	S(Si-O)
		965	S(Si-O)
		980	S(Si-O)

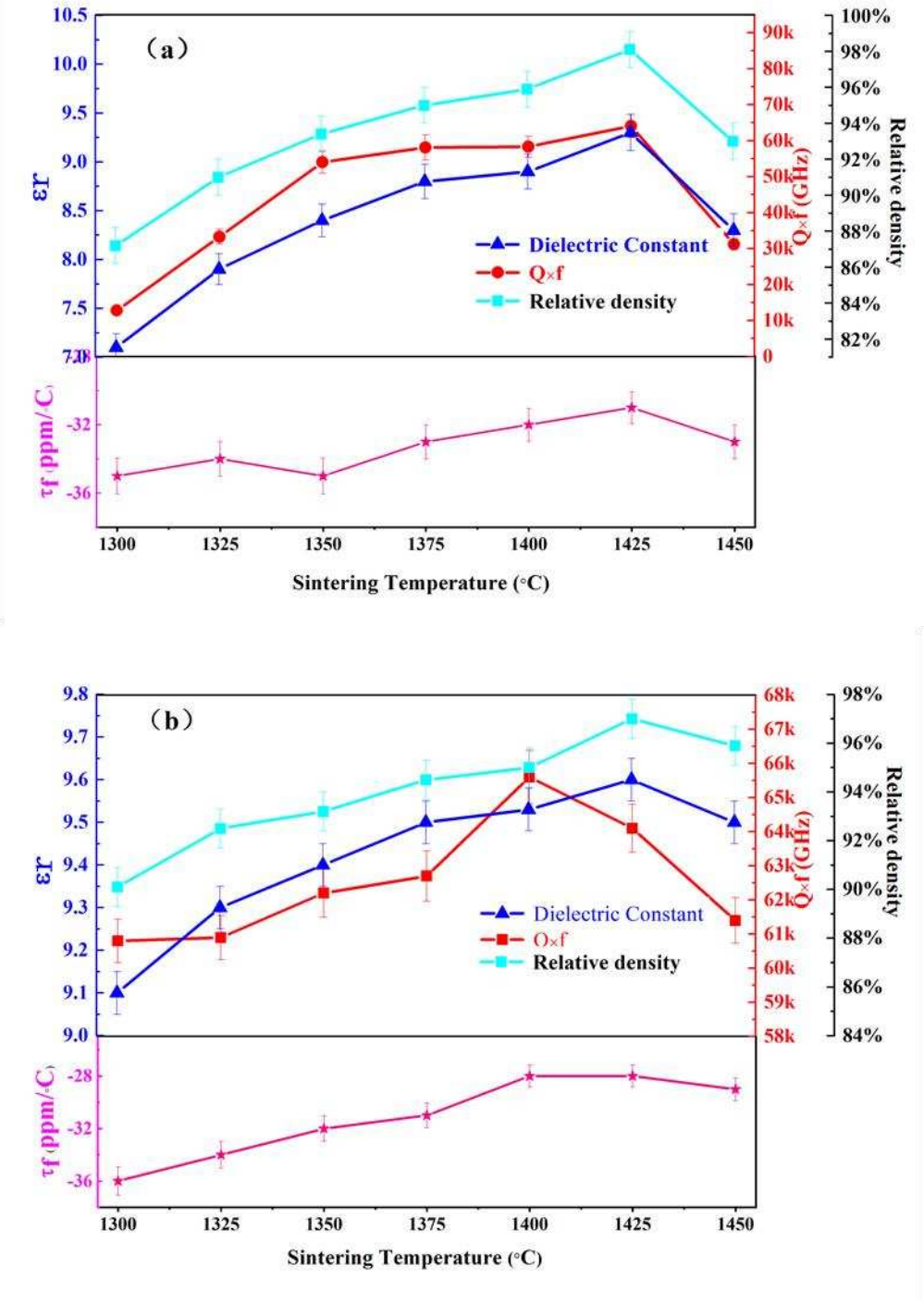

Fig.4, Microwave dielectric properties and relative density of (a) $SrY_2Si_3O_{10}$ and (b) $BaY_2Si_3O_{10}$ ceramics sintered at different temperatures.

The microwave dielectric properties and relative density of $AY_2Si_3O_{10}$ (A=Sr, Ba) ceramics as a function sintering temperature are plotted in Fig. 4. $AY_2Si_3O_{10}$ (A=Sr, Ba) ceramics have a broader range of densification temperature (above 100°C) to obtain >95% relative density. ε_r, Qf and τ_f of $SrY_2Si_3O_{10}$ and $BaY_2Si_3O_{10}$ increase with increase of sintering temperature, and then decrease after reaching optimum values. The optimum microwave dielectric properties are ε_r = 9.3, Qf = 64100GHz, τ_f= -31ppm/°C for $SrY_2Si_2O_{10}$ and ε_r = 9.5, Qf = 65600GHz, τ_f = -28ppm/°C for $BaY_2Si_2O_{10}$ sintered at 1425°C and 1400°C, respectively.

The Qf are mainly determined by intrinsic factors such as inharmonic factors like polarization, as well as extrinsic factors such as grain size, porosity, grain boundary and point defects.[30] Here, the enhancement of Qf is mainly attributed to the reduction of porosity (Fig. 4) and the distribution of grain size (Fig. 2). Similar to Qf, ε_r of $AY_2Si_3O_{10}$ (A=Sr, Ba) ceramics also varies with relative density. Hence, ε_r is corrected by the Bosman and Havinga formula to eliminate the influence of porosity: [31]

$$\varepsilon_c = \varepsilon_m(1+1.5P) \quad (2)$$

$$P = (1-\rho_r) \quad (3)$$

Where, ε_c and ε_m are the corrected and measured ε_r, P is porosity and ρ_r is relative density. ε_c are 9.6 and 9.8, near to the measured values of 9.3 and 9.6 for $SrY_2Si_3O_{10}$ and $BaY_2Si_3O_{10}$ ceramics, respectively.

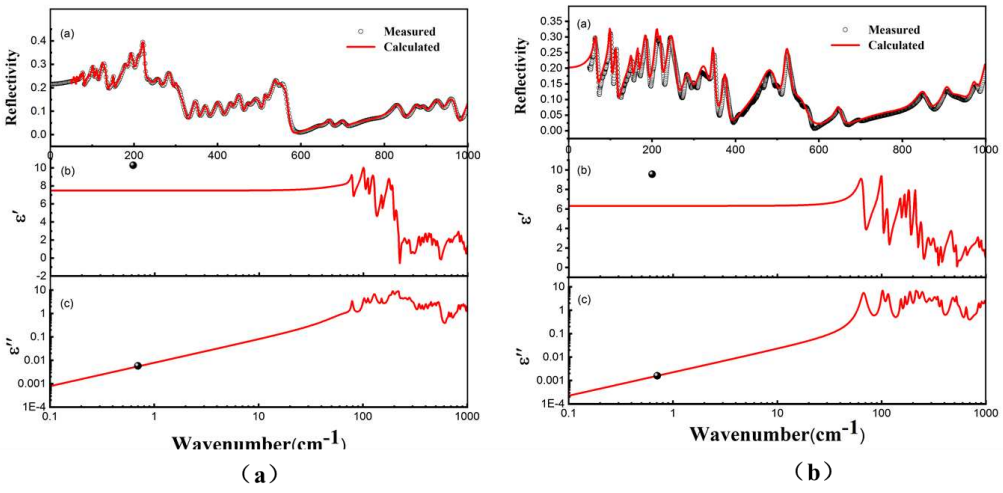

Fig. 5, the measured and calculated infrared reflectivity spectra and the real and imaginary

parts of the complex responses obtained from the fitting of the IR reflectivity spectra (the black circles are the measured values in microwave region) of (a) $SrY_2Si_3O_{10}$ and (b) $BaY_2Si_3O_{10}$.

The intrinsic microwave dielectric properties of $AY_2Si_3O_{10}$ (A=Sr, Ba) ceramics were further investigated by the IR reflectivity, as shown in Fig. 5, the data for which were analyzed using a classical harmonic oscillator model as follows: [32,33]

$$\varepsilon^*(\omega)=\varepsilon'(\omega)-i\varepsilon''(\omega)=\varepsilon_\infty+\sum_{j=1}^{n}\frac{\omega_{pj}^{\ 2}}{\omega_{oj}^{\ 2}-\omega^2-j\omega\gamma_j} \tag{4}$$

Where, n is the sequence of polar-phonon modes. ω_{pj}, ω_{oj}, and γ_j are the plasma frequency, eigenfrequency, and damping constant of the j-th mode, respectively. $\varepsilon^*(\omega)$ is the complex dielectric function. ε_∞ is the ε_r caused by the electronic polarization at high frequencies. The complex reflectivity R (ω) can be regarded as:

$$R(\omega)=\left|\frac{\sqrt{\varepsilon^*(\omega)}-1}{\sqrt{\varepsilon^*(\omega)}+1}\right|^2 \tag{5}$$

$\varepsilon'(\omega)$ and $tan\delta$ can be converted to:

$$\varepsilon'(\omega)=\varepsilon_\infty+\sum_{j=1}^{n}\Delta\varepsilon_j'=\varepsilon_\infty+\sum_{j=1}^{n}\frac{\omega_{pj}}{\omega_{oj}^{\ 2}} \tag{6}$$

$$\tan\delta=\frac{\varepsilon''(\omega)}{\varepsilon'(\omega)}=\sum_{j=1}^{n}\frac{\Delta\varepsilon_j\gamma_j}{\omega_{oj}^{\ 2}\left(\varepsilon_\infty+\sum_{j=1}^{n}\Delta\varepsilon_j\right)}\approx\sum_{j=1}^{n}\frac{\omega}{\varepsilon'(\omega)}\frac{S_j\gamma_j}{\omega_j^4} \tag{7}$$

Where, $\triangle\varepsilon_j$ is the photonic contribution to the permittivity from the j-th Lorentz oscillator. According to the factor group analysis of triclinic and monoclinic structures with $P\bar{1}$ and $P2_1/m$ space groups, the IR active modes of $SrY_2Si_3O_{10}$ and $BaY_2Si_3O_{10}$ are described as $48A_u$ and $22A_u+26B_u$, respectively. The IR reflectivity values are listed in Table 5 and Table 6. According to the fitted parameters, the calculated ε_r of $SrY_2Si_3O_{10}$ and $BaY_2Si_3O_{10}$ are 1.68 and 1.97 at optical and 5.8113 and 4.3487 at microwave frequencies, respectively. These values are significantly lower than those measured (9.3 and 9.5, respectively), which could be due to extrinsic contributions stemming from defects.[34-36] The contributions of the optical dielectric constant are 38.6% and 33.9%, respectively, compared to the total permittivity, suggesting that the microwave properties are dominated by ionic rather than electronic polarization [37]. The vibrational modes below 350cm^{-1} of $AY_2Si_3O_{10}$ (A=Sr, Ba) ceramics contribute

3.0124×10^{-4} and 1.4968×10^{-4} to the dielectric loss, accounting for 79.12% and 68.14% of the total loss, respectively. This effect may be explained by considering $\triangle\tan\delta_j$ is positively related to $\omega S_j\gamma_j\omega_j^{-4}$, and decreases sharply with increasing ω_j.[38]

Table. 5, Phonon parameters obtained from the fitting of the infrared reflectivity spectra of $SrY_2Si_3O_{10}$ ceramics

Mode	ω_{oj} (cm^{-1})	ω_{pj} (cm^{-1})	γ_j (cm^{-1})	$\triangle\varepsilon_j$	$\triangle\tan\delta_j$ ($\times10^{-4}$)
1	74.785	53.413	54.774	0.51	0.732
2	79.07	26.143	3.4523	0.109	0.0437
3	103.07	46.036	6.3615	0.199	0.0617
4	112.06	37.806	4.7608	0.114	0.0425
5	129.08	98.485	13.613	0.582	0.105
6	151.34	32.284	3.5816	0.0455	0.0237
7	157.76	107.74	54.08	0.466	0.343
8	180.63	95.681	15.055	0.281	0.0833
9	194.17	117.32	12.092	0.365	0.0623
10	211.57	153.61	18.823	0.527	0.089
11	220.15	85.042	8.007	0.149	0.0364
12	230.87	134.8	262.63	0.341	1.14
13	235.99	73.199	16.807	0.0962	0.0712
14	255.52	171.12	35.372	0.448	0.138
15	280.66	114.71	18.929	0.167	0.0674
16	302.61	151.47	38.67	0.251	0.128
17	347.16	95.352	14.987	0.0754	0.0432
18	371.42	91.373	16.059	0.0605	0.0432
19	402.15	137.3	24.25	0.117	0.0603
20	431.94	101.05	17.031	0.0547	0.0394
21	451.28	135.28	18.301	0.0899	0.0406
22	473.28	83.639	15.489	0.0321	0.0327
23	491.79	174.14	29.808	0.125	0.0606
24	514.78	90.842	11.264	0.0311	0.0219
25	526.83	100.65	16.57	0.0365	0.0315
26	535.99	133.73	19.333	0.0623	0.0361
27	551.93	104.57	21.928	0.0359	0.0397
28	644.52	68.547	28.342	0.0113	0.044
29	670.23	92.374	18.108	0.019	0.027
30	701.82	95.313	21.133	0.0184	0.0301
31	777.4	209.06	90.176	0.0723	0.116
32	831.32	221.99	34.158	0.0713	0.0411
33	875.93	164.82	24.776	0.0354	0.0283

34	893.65	134.28	23.626	0.0226	0.0264
35	923.25	250.06	37.714	0.0734	0.0408
36	956.42	184.73	26.709	0.0373	0.0279
37	1002.7	200.62	28.424	0.04	0.0283
38	1034.5	204.78	32.532	0.0392	0.0314
$SrY_2Si_3O_{10}$	ε_∞=1.68		ε_0=5.8113		$\sum_{\triangle tan\delta j}$=4.058

Table. 6 Phonon parameters obtained from the fitting of the infrared reflectivity spectra of $BaY_2Si_3O_{10}$ ceramics

Mode	ω_{oj} (cm^{-1})	ω_{pj} (cm^{-1})	γ_j (cm^{-1})	$\triangle\varepsilon_j$	$\triangle tan\delta_j$ ($\times10^{-4}$)
1	67.554	54.068	7.9449	0.641	0.118
2	102.15	63.394	6.0099	0.385	0.0588
3	115.48	63.061	7.5015	0.298	0.065
4	153.21	48.374	5.9034	0.0997	0.0385
5	168.28	51.741	5.0153	0.0945	0.0298
6	175.11	53.022	12.76	0.0917	0.729
7	187.24	110.01	11.288	0.345	0.0603
8	213.82	99.51	8.7921	0.217	0.0411
9	221.44	81.254	8.3085	0.135	0.0375
10	246.14	173.87	22.622	0.499	0.0919
11	287.41	126.27	26.151	0.193	0.091
12	324.35	189.04	35.884	0.34	0.111
13	346.1	85.2	8.612	0.0606	0.0249
14	374.75	101.14	12.862	0.0728	0.0343
15	482.84	264.46	46.424	0.3	0.0961
16	522.03	142.85	14.664	0.0749	0.0281
17	553.78	168.64	54.153	0.0927	0.0978
18	649.77	122.17	21.367	0.0354	0.0329
19	785.11	208.22	148.6	0.0703	0.189
20	853.12	196.47	31.676	0.053	0.0371
21	936.54	331.41	81.159	0.125	0.0867
22	908.5	146.51	22.906	0.026	0.0252
23	972.08	131.98	18.534	0.0184	0.0191
24	1068.5	69.246	18.573	0.0042	0.0174
25	999.94	276.48	36.312	0.0765	0.0363
$BaY_2Si_3O_{10}$	ε_∞=1.97		ε_0=4.3487		$\sum_{\triangle tan\delta j}$=2.196

4. Conclusions

The $SrY_2Si_3O_{10}$ and $BaY_2Si_3O_{10}$ microwave dielectric ceramics with low ε_r have been prepared by solid-state reaction. Rietveld refinement of XRD data revealed that $SrY_2Si_3O_{10}$ and $BaY_2Si_3O_{10}$ belong to the triclinic and monoclinic systems with space groups $P\bar{1}$, and $P2_1/m$, respectively. Due to low crystal symmetry, grains of $SrY_2Si_3O_{10}$ and $BaY_2Si_3O_{10}$ display a plate and pill morphologies. The grain size increased with increasing sintering temperature. The modes with Raman shift below $350cm^{-1}$ are dominated by O-Y-O bending modes. The region from 350 cm^{-1} to $650cm^{-1}$ are dominated by O-Si-O bending modes, and > $800cm^{-1}$ is assigned to Si-O stretching modes. The intrinsic (static) dielectric properties of the samples were calculated using the 4-P model based on far-IR reflectance spectroscopy. The best microwave dielectric properties of $SrY_2Si_3O_{10}$ and $BaY_2Si_3O_{10}$ ceramics sintered 4h at 1425°C and 1400 °C were ε_r= 9.3, Q×f= 64100GHz, τ_f= -31ppm/°C and ε_r= 9.5, Q×f= 65600GHz, τ_f = -28ppm/°C, respectively. Their low cost, easy preparation and excellent microwave dielectric properties suggest that $ASrY_2Si_3O_{10}$ (A=Sr, Ba) ceramics are promising candidates for 5G applications, provided τ_f can be further tuned toward zero.

Conflicts of interest

There are no conflicts to declare

Acknowledgements

This work was supported by the National Natural Science Foundation of China under grant number 51672063 and 51802062. Open projects of Key Laboratory of inorganic functional materials and devices, Shanghai silicate institutes, Chinese academy of sciences under grant number: KLIFMD201708. The authors would like to thank the administrators in IR beamline workstation (BL01B) of National Synchrotron Radiation Laboratory (NSRL) for their help in the IR measurement. Dr Wang and Professor Reaney acknowledge the support of Engineering and Physical Science Research Council grants, EP/N010493/1 and EP/L017563/1

Notes and references

[1]J. Zhang, Z. X. Yue, Y. Y. Zhou, X. H. Zhang and L. T. Li, J. Am. Ceram. Soc. 2015, 98, 1548-1554.

[2]J. X. Bi, C. F. Xing, Y. H. Zhang, C. H. Yang and H. T. Wu, J. Alloys. Compd. 2017, 727, 123-134.

[3]J. E. F. S. Rodrigues, P. J. Castro, P. S. Pizani, W. R. Correr and A. C. Hernandes, Ceram. Int. 2016, 42, 18087-18093.

[4] J. Zhang, Y. Luo, Z. X. Yue and L. T. Li, J. Am. Ceram. Soc. 2018, 102, 342-350.

[5] Z. Y. Zou, Z. H. Chen, X. K. Lan, W. Z. Lu, B. Ullah, X. H. Wang and W. Lei, J. Eur. Ceram. Soc. 2017, 37, 3065-3071.

[6] H. F. Zhou, X. H. Tan, J. Huang, N. Wang, G. C. Fan and X. L. Chen, J. Alloys. Compd. 2017, 696, 1255-1259.

[7] H. C. Xiang, L. Fang, W. S. Fang, Y. Tang and C. C. Li, J. Eur. Ceram. Soc. 2017, 37, 625-629.

[8] J. B. Song, K. X. Song, J. S. Wei, H. X. Lin, J. Wu, J. M. Xu, W. T. Su and Z. Q. Cheng, J. Am. Ceram. Soc. 2018, 101, 244-251.

[9] H. S. Ren, L. Hao, H. Y. Peng, M. Z. Dang, T. Y. Xie, Y. Zhang, S. H. Jiang, X. G. Yao, H. X. Lin and L. Luo, J. Eur. Ceram. Soc. 2018, 38, 3498-3504.

[10]J. Guo, D. Zhou, H. Wang, Y. Chen, Y. Zeng, F. Xiang, Y. Wu and X. Yao, J. Am. Ceram. Soc. 2012, 95, 223-237.

[11]S. P. Wu, C. Jiang, Y. X. Mei and W. P. Tu, J. Am. Ceram. Soc. 2012, 95, 37-40.

[12] K. Kakimoto, T. Tsunooka, H. Osato, H. Sugiyama, H. Ogawa, K. Kakimoto and H. Tsunooka, J. Ceram. Soc. Jpn. 2004, 112, 1637-1640.

[13] Y. Guo, H. Ohsato and K. I. Kakimoto, J. Eur. Ceram. Soc. 2006, 26, 1827-1830.

[14] S. H. Kweon, M. R. Joung, J. S. Kim, B. Y. Kim, S. Nahm and J. H. Paik, J. Am. Ceram. Soc. 2011, 94, 1995-1998.

[15] S. P. Wu, D. F. Chen, C. Jiang, V. X. Mei and Q. Ma, Mater. Lett. 2012, 91, 239-241.

[16] I. J. Induja and M. T. Sebastian, J. Eur. Ceram. Soc. 2017, 37, 2143-2147.

[17] K. X. Song, P. Liu, W. T. Su, H. X. Lin, W. T. Su, H. B. Qin, J. Wu, Z. H. Ying and J. Liang, J. Eur. Ceram. Soc. 2015, 36, 1167-1175.

[18] Atlas L. J. Ceram, 1952, 60(2): 125-147.

[19] E. F. Michael and X. Y. Liu, J. Solid. State. Chem. 2001, 161, 166-172.

[20] J. W. Jeffery and P. F. Lindley, Nature. 1973, 241, 42-43.

[21]A. S. Povarennykh, B. N. Litvin and M. Bednar, Geologicheskii. Zhurnal. 1976, 36, 76-85.

[22] M. W. Wieczorek, U. Kolitsch and E. Tillmanns, Eur. J. Mineral. 2010, 22, 245-258.

[23] U. Kolitsch, M. Wierzbicka and E. Tillmanns, Acta. Crystallogr. D. 2007, 62, 97-99.

[24] Z. G. Xia, Y. J. Liang, W. Z. Huang, D. Y. Yu, M. F. Zhang and M. H. Tong, Ceram. Int. 2013, 39, 7097-7100.

[25] B. H. Toby, J. Appl. Cryst. 2001, 34, 210-213.

[26] B. W. Hakki and P. D. Coleman, IEEE. Trans. Microw. Theory. Technol. 1960, 8, 402-410.

[27] E. Kroumova, M. Aroyo, J. P. Mato, A. Kirov, C. Capillas, S. Ivantchev and H. Wondratschek, A. Multinational. Journal. 2003, 76, 155-170.

[28]A. Orera, E. Kendrick, D. C. Apperley, V. M. Orera and P. R. Slater, Dalton. T. 2008, 39, 5296-5301.

[29] E. Arroyabe, F. Prechtel, D. M. Többens, R. Kaindl and V. Kahlenberg, Eur. J. Mineral. 2011, 23, 425-435.

[30] S. D. Ramarao, S. R. Kiran and V. R. K. Murthy, J. Mater. Res. Bull. 2014, 56, 71-79.

[31] S. H. Yoon, D. W. Kim, S. Y. Cho and K. S. Hong, J. Eur. Ceram. Soc. 2006, 26, 2051-2054.

[32] D. Zhou, L. Pang, D. Wang and I. M. Reaney, J. Mater. Chem. C. 2018, 6, 9290-9313.

[33] C. Xing, J. Li, J. Wang, H. Chen and F. Shi, Inorg. Chem. 2018, 57, 7121-7128.

[34] Liu B, Liu X Q and Chen X M. J. Mater. Chem. C, 2016, 4(8): 1720-1726.

[35] Liu B, Li L, Liu X Q, et al. J. Mater. Chem. C, 2016, 4(21): 4684-4691.

[36] Yi L, Liu X Q and Chen X M. Int. J. Appl. Ceram. Tec, 2015, 12: E33-E40.

[37] H. C. Yang, S. R. Zhang, H.Y. Yang, Y. Yuan and E. Z. Li, Dalton. T. 2018, 47, 15808-15815.

[38] X. C. Fan, X. M. Chen and X. Q. Liu, Chem. Mater. 2008, 20, 4092-4098.